GEORGIA INSTITUTE OF TECHNOLOGY

Nematic Order in Spherical Geometries

by

Sharan Devaiah

An Undergraduate Thesis Submitted in Partial Fulfillment of the Requirements for the Research Option

in the

School of Physics

May 2010

Nematic Order in Spherical Geometries

An Undergraduate Thesis Submitted in Partial Fulfillment of the Requirements for the Research Option in Physics

Approved By,

Dr. Alberto Fernandez-Nieves, Advisor

Dr. Venkata Gundabala, Second Reader

Dr. Brian Kennedy, Associate Chair for Undergraduate Studies

Acknowledgements

I wish to thank my advisor, Dr. Alberto Fernandez-Nieves, for letting me join his group, and for his guidance and support. Working with him has been an absolute pleasure, and if it weren't for his infectious passion and enthusiasm for his research, the work presented in this thesis would scarcely have been achieved.

I also wish to thank my fellow group member, Teresa Lopez-Leon, for training me in microfluidics.

Finally, I would like to thank my family for all their support. Thanks to them, I have been able to afford an education at Georgia Tech.

GEORGIA INSTITUTE OF TECHNOLOGY

Abstract

School of Physics

Bachelor of Science in Physics

by Sharan Devaiah

Nematic Liquid crystals (NLC) are rod like molecules that in the absence of external influences arrange themselves parallel to each other and hence tend to point in a given direction. The average orientation of these molecules is given by the director **n**, which is essentially a bi-directional vector which quantifies the orientation of the molecules in a given region of the sample. When NLCs are confined to a curved surface, the geometrical constraints imposed by the surface causes a distortion in the molecular orientation. In certain regions, the molecular orientation is such that the director cannot be defined. Such regions are called topological defects. Theory had predicted that the ground state of NLCs confined to a spherical surface has four defects located at the vertices of a tetrahedron[1]. The tetrahedal defect structure is of great interest in material science because defects in NLCs are regions that can be functionalized to serve as *bonds* that could pave the way for making macroatoms with tetrahedral bonding properties similar to sp^3 hybridized atoms like Carbon[2]. By using ultrathin shells of NLCs, we show that the tetrahedral structure is indeed what we observe experimentally, verifying the theory for the first time. However, this tetrahedral structure coexists with other structures consisting of two or three defects. We also study these defect structures.

Contents

List of Figures

Chapter 1

Introduction and Literature Review

1.1 Introduction

The study of liquid crystals in confined geometries has been motivated by various technological applications, in addition to serving as a fascinating playground for physicists and mathematicians interested in applications of geometrical and topological ideas to material science[3]. In confined geometries, the liquid crystal ground state results from a competition between the elastic energies of the system and the geometrical constraints that need to be satisfied.

Lubensky and Prost showed that a two dimensional layer of nematic liquid crystals confined to the surface of a sphere should give rise to four *defects* in the molecular ordering[1]. Due to the elastic energies associated with these defects, they predicted that the defects should repel each other and move away as far as possible, situating themselves at the vertices of a tetrahedron. Based on this prediction, Nelson suggested that by coating spherical particles with a thin layer of nematic liquid crystal and functionalizing these defects by attaching ligands, which could serve as linkers, to these points, one could fabricate tetravalent colloidal particles similar to sp^3 hybridized atoms like Carbon[2]. Instead of being on the angstrom scale, these particles would be on the micron scale, having fascinating optical properties in the visible range of the electromagnetic spectrum.

Though the theoretical prediction about the tetrahedral arrangement has been around for several years, the theory was lacking an experimental verification. Attempts to verify the theory by creating thin nematic liquid crystal shells showed that these thin shells

do indeed have four defects, but these defects were not in the expected tetrahedral arrangement[4].

In this thesis, we show that for sufficiently thin nematic liquid crystal shells, the defects are indeed located at the vertices of a tetrahedron. We do this by creating identical shells and then performing ensemble averages to quantify the locations of the defects. This, in effect, is the first experimental verification of Lubensky and Prost's theory. We also study shells that have two or three defects in order to quantify the arrangement of defects on such shells.

1.1.1 Geometrical Frustration

Geometrical frustration refers to situations where the preferred local order, favored by the physical interaction among the constituents of the system, cannot propagate throughout the system due to geometrical constraints imposed by the substrate.

A commonplace example of a frustrated system is a magnetic system where antiferromagnetically interacting spins are located on a triangular lattice. Since these spins tend to antialign, when they are located on a square lattice (see Fig. 1.1(a)), each pair can antialign with all its neighbors. When, however, they are located on a triangular lattice (see Fig. 1.1(b)), the third spin cannot simultaneously antialign itself with the other two spins, and the system is frustrated.

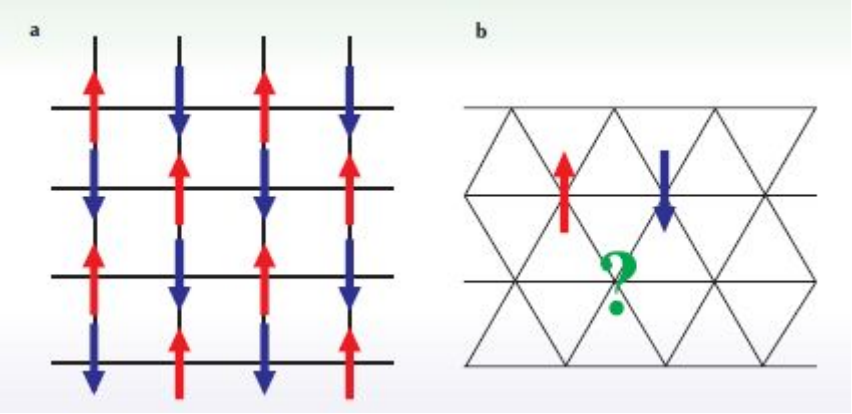

FIGURE 1.1: [1]A geometrically frustrated system is one in which the lattice precludes the simultaneous minimization of all interactions. (a) In the unfrustrated antiferromagnet on the square lattice, each spin can be antialigned with all its neighbors. (b) On a triangular lattice, such an arrangement is impossible: Three neighboring spins cannot be pairwise antialigned, and the system is frustrated.

Let us now consider the problem of packing identical particles on a flat 2 dimensional surface. In this case, the particles pack in a triangular lattice with each particle having 6 neighbors. Such a structure is a two-dimensional crystal with six-fold local order. If

the packing is attempted on a closed surface, the interplay between geometry and order can be understood through the Euler theorem of topology [6] that relates the number of vertices V, edges E and faces F when a two-manifold surface M is tiled with regular polygons:

$$V - E + F = \chi, \tag{1.1}$$

where χ is the Euler characteristic of M. It can be shown that $\chi = 2(1-g)$, where g, the genus of M, equals the number of *handles* M has. For instance, a sphere has no *handles* and thus $g = 0$ while a torus has one *handle* and thus $g = 1$. Thus, a sphere has $\chi = 2$, while a torus has $\chi = 0$. Two closed surfaces with the same Euler characteristic, and hence the same genus, can be continuously deformed from one to the other. For example, a coffee mug (a closed surface with one handle) can be continuously deformed to take the shape of a torus, and hence they are topologically equivalent. A torus, however, cannot be smoothly deformed into a sphere, and hence a torus and a sphere are not topologically equivalent.

In the case of crystals constrained to curved surfaces, there could be regions where the six-fold order is not present. These regions are topological defects, which are characterized by their *topological charge* q_i. The topological charge establishes the departure in coordination number from the value of 6 characteristic of a planar triangular lattice: $q_i = 6 - c_i$, where c_i is the coordination number of the ith vertex.

Consider a tiling of n-sided polygons where k faces meet at each vertex. Since each edge is shared between two faces and links two vertices it follows that

$$nF = 2E = \sum_k kV_k \tag{1.2}$$

where V_k is the number of vertices of degree k. For a 2D crystal with a triangular lattice it follows from Eq. 1.1 that

$$Q = \sum_{i=1}^{V} q_i = 6\chi. \tag{1.3}$$

For a sphere ($\chi = 2$), Eq.1.3 implies that any triangulation will contain defects such that the total topological charge of the lattice Q = 12 (see Fig. 1.2). A spherical crystal with a triangular lattice can, for example, satisfy this condition by having 12 five-fold vertices ($q_i = 1$) in an otherwise ordered network of six-fold vertices. This kind of structure is seen, for example, in the fullerene structure of carbon or in an ordinary soccer ball, which is made up of 12 pentagonal patches embedded in a network of hexagonal patches. These

FIGURE 1.2: Defects on a sphere. (Left) Twelve $q = 1$ defects on a spherical crystal with a triangular lattice. (Center) Five-fold defect on a triangular lattice in a region of positive Gaussian curvature. (Right) Defects (pentagons) on a soccer ball.

12 defects, which are suppressed in a planar arrangement, result from the geometrical frustration associated with the topology of a sphere.

1.2 Nematic Liquid Crystals

Nematic Liquid Crystals (NLC) are rod shaped molecules that have local orientational order, but no positional order. Hence, they are able to flow like a liquid while still possessing some properties of crystals (which have both orientational and positional order), but even as they flow, on a local scale, the molecules tend to point in the same average direction. This local orientation is characterized by the director, $\pm\mathbf{n}$, as shown in Fig. 1.3.

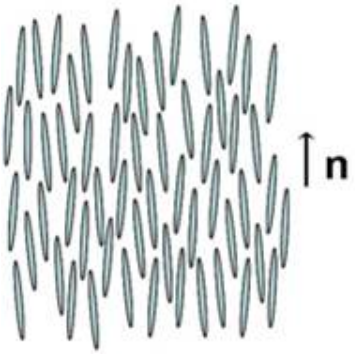

FIGURE 1.3: Schematic of Nematic Liquid Crystals.

The NLC that we use in our experiments is 4-cyano-4-n-pentylbiphenyl (5CB). It is convenient to work with it since it is in the nematic phase at room temperature, as shown by the phase diagram in Fig. 1.4. The rod shaped molecules that make up 5CB are strongly anisometric elongated molecules. The inner part of these molecules is rigid (phenly groups) and the outer part flexible (aliphatic chains). This double

character leads to interactions that give rise to the orientational order and the fluidity characteristic of the nematic phase.

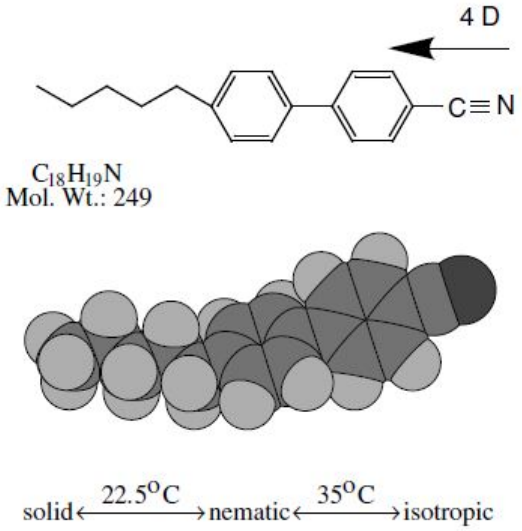

FIGURE 1.4: Molecular structure and phase diagram of 4-cyano-4-n-pentylbiphenyl(5CB).

1.2.1 Free Energy of the Nematic Phase

The ground state of a NLC is a spatially uniform director field, and any deviation from this increases the energy of the system. This is given by the Frank-Oseen free energy density[7],

$$f_{el} = \frac{1}{2}[K_1(div\mathbf{n})^2 + K_2(\mathbf{n}\cdot curl\mathbf{n})^2 + K_3(\mathbf{n}\times curl\mathbf{n})^2], \tag{1.4}$$

where K_1, K_2, and K_3 are the *splay*, *twist*, and *bend* elastic constants, respectively. These elastic constants are measures of the different ways in which the nematic can be distorted from its uniform director configuration, as shown in Fig. 1.5.

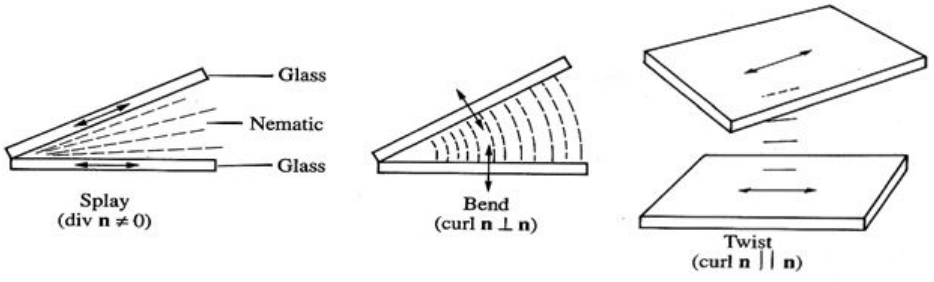

FIGURE 1.5: Illustration of the characteristic deformations in a nematic liquid crystal: *splay, twist, and bend.*

As can be seen from Eq. 1.4, the transformation $\mathbf{n} \rightarrow -\mathbf{n}$ does not change the energy. Furthermore, any distortion in a nematic liquid crystal can be understood as any combination of pure splay, pure twist, and pure bend. In the one-constant approximation, where $K = K_1 = K_2 = K_3$, the Frank-Oseen free energy takes the simpler form:

$$f_{el} = \frac{1}{2}K((div\mathbf{n})^2 + (\mathbf{n} \times curl\mathbf{n})^2) \tag{1.5}$$

1.2.2 Topological Defects in Nematics

Topological defects in NLCs are spatial regions, either points, lines or walls, where the orientational order parameter, i.e. the director, is not defined [7].

Topological defects arise as a consequence of broken continuous symmetry[8], and are found in disparate branches of physics such as crystalline solids[9], liquid crystals, quantum Hall fuilds[10], and also in certain cosmological models[11]. For instance, dislocations in crystalline solids are examples of topological singularities since at these points the symmetry of translation is broken along a line.

In nematic liquid crystals, two types of defects are found: point defects, and line defects, which are also called disclinations. A descriptive approach to the classification of defects in nematics is inspired by the Volterra process for dislocations in crystalline solids[12]. Disclinations distort order in the whole volume of the system, and this distortion can be figured out by the extent by which the order parameter rotates when a full circle is traversed around the defect.

The construction of a defect using the Volterra process is illustrated in Fig. 1.6. In the Volterra process, a surface Σ in the nematic, such as that shown in Fig. 1.6(a), is cut open by an angle π, and extra nematic material is introduced in this gap, as shown in Fig. 1.6(b). Then, the nematic is allowed to relax, yielding the structure shown in Fig. 1.6(c). The topological charge q of this defect is the ratio $q = \alpha/2\pi$, where α is the angle by which the director rotates after traversing a circular path, called the Burgers circuit, around the defect. The sign of α is determined by comparing the direction in which the Burgers circuit is traversed and the hodograph Γ of the directors shown in Fig.1.6(d). The hodograph is constructed by parallel-transporting each director that is met when traversing the Burgers circuit γ to an origin $\mathbf{O}$. In the example shown in Fig. 1.6, the Burgers circuit and the hodograph are oriented in opposite directions, and hence the sign of α is negative, and the disclination produced has $q = -1/2$. In this example, a wedge of matter was introduced during the Volterra process. If, instead, the same amount of matter is removed from the wedge, a disclination of $q = +1/2$ is produced.

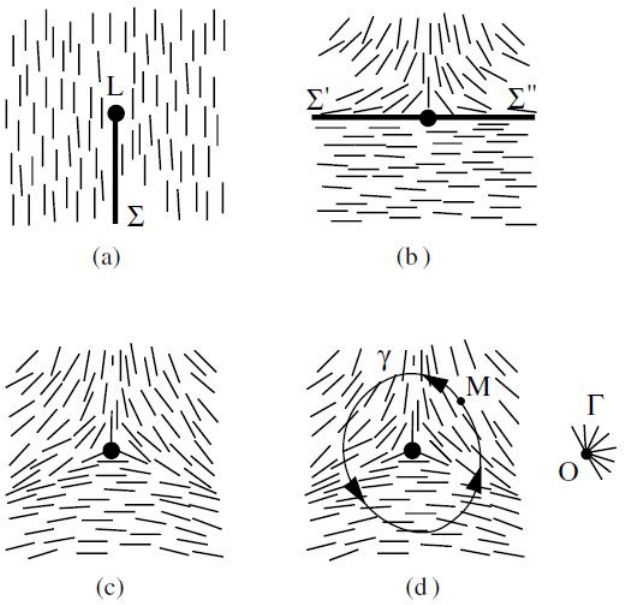

FIGURE 1.6: Volterra process for a $q = -1/2$ disclination in a nematic: (a) cut surface Σ at a line **L**,(b) opening of the lips of Σ by an angle π and introduction of extra matter, (c) elastic relaxation, (d) the Burgers circuit γ and its hodograph Γ.

In a similar manner, disclinations of different strengths can be generated, and some examples of disclinations found in nematics are shown in Fig. 1.7.

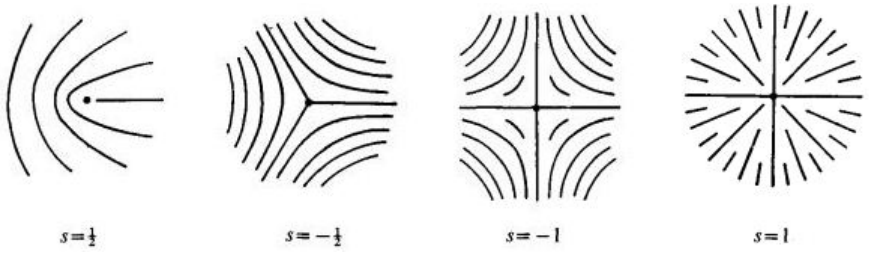

FIGURE 1.7: Topological defects of strenghts $\pm\frac{1}{2}$ and ± 1

Since the region surrounding a defect is distorted, the energy of the nematic in this region is greater than the ideal spatially uniform conformation. The configuration of the director field around a disclination is a result of the minimization of the Frank-Oseen free energy (Eq.1.4). In the one-constant approximation the energy F_d in the presence of a disclination is given by

$$F_d = E_c + \pi K q^2 ln\frac{R}{r_c}, \tag{1.6}$$

where E_c is the energy of the defect core, R is the size of the sample, and r_c is the cutoff radius of the defect core[7].

1.2.3 Optical Properties of Nematic Liquid Crystals

Nematic liquid crystals are birefringent in nature. When linearly polarized light passes through a birefringent medium, its component in the direction of the director , the extraordinary wave, has a refractive index n_e, and its component perpendicular to the director, the ordinary wave, has a refractive index n_0. Since the two waves have different refractive indices, they travel with different velocities in the medium, and hence, take different times to pass through the sample. Consequently, when the wave exits the medium, there is a phase shift, making the emergent wave elliptically polarized. Now, if an analyzer, which is a linear polarizer oriented perpendicular to the polarizer, is placed on the other side of the birefringent sample, since the emergent wave is elliptically polarized, it is not extinguished by the analyzer. If however, the linearly polarized light that impinges on the sample is polarized either perpendicular or parallel to the director, then, since there is only one wave traveling through the medium and consequently no phase shift, the light that emerges from the medium remains linearly polarized and hence is completely extinguished by the analyzer (see Fig. 1.8).

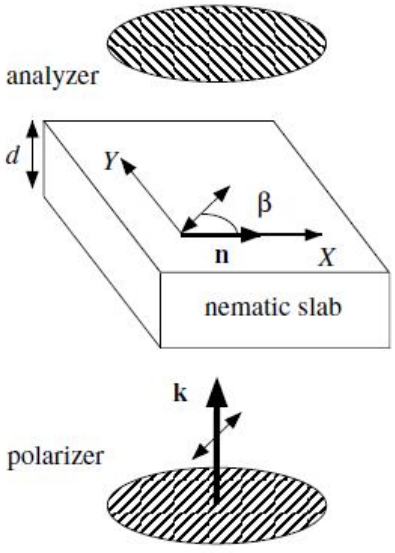

FIGURE 1.8: Crossed Polarizers with a nematic sample in between them

The intensity of the light that emerges from the crossed polarizer setup is given by [12]:

$$I = I_0 \sin^2(2\beta) \sin^2 \left[\frac{\pi d}{\lambda_0} (n_e - n_o) \right] \tag{1.7}$$

Where I_0 is the intensity of the light that impinges on the sample, β is the angle between the polarization direction of the incident light and the director, d is the thickness of the

nematic sample, λ_0 the wavelength of the incident light, and n_e and n_o the refractive indices of the extraordinary and the ordinary waves respectively.

When a sample of NLCs is sandwiched between two cover slips and observed under a microscope fitted with crossed polarizers, one often observes the texture shown below, called the Schleiren texture.

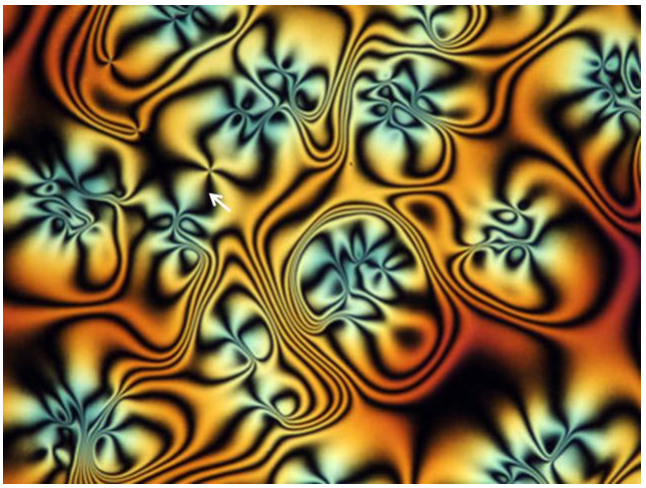

FIGURE 1.9: Schlieren texture of a thin film of NLC. Dark brushes mark the regions where the director is either parallel or perpendicular to the polarizer.

This texture can be understood via Eq. 1.7. Firstly, it should be noted that though the molecules of NLCs tend to align along a given direction, in general, the orientation of the molecules is not the same throughout a sample because the ideal conformation will not be compatible with the constraints imposed by the limiting surfaces (eg. cover slip surfaces) or by external fields acting on the molecules. Since the phase shift, and thus, I depend on λ_0, when the sample is illuminated with white polarized light, one sees a colorful texture. In regions where the director is either parallel or perpendicular to the polarizer, no light comes through the analyzer, and hence, these regions (called brushes) appear dark. Points at which the brushes converge are centers of topological defects. These are singularities where the director cannot be defined.

The topological charge of disclinations in nematics can be visually identified by quantifying the number of brushes emerging from it. The charge is given by $q = \frac{1}{4} \times$ *number of brushes*. The sign of the charge can be determined by rotating the crossed polarizers. When this is done, the centers of the defects do not change, but the brushes themselves rotate because the orientation of the director changes continuously about the disclinations. If the brushes rotate in the direction in which the crossed polarizers are rotated, then these disclinations have positive sign. If the brushes rotate in the opposite directions, then the disclinations associated with them have negative sign. In nematics, only disclinations of strengths $\pm\frac{1}{2}$ and ± 1 are usually observed.

1.3 Nematic Order on the surface of a sphere

Eq. 1.3 is a special case of geometrical frustration on a two manifold surface where the local orientations are defined modulo $2\pi/c = \pi/3$[2], since $c = 6$. In general, one can consider a p-attic director field for which the local orientations are defined modulo $2\pi/p$. The topological charge of a disclination in this case is $q = \Delta\theta/(2\pi)$, where $\Delta\theta$ is the angle the director rotates in one counter-clockwise circuit of any closed contour enclosing the defect. Eq. 1.2 then becomes

$$Q = \sum_{i=1}^{N} q_i = p\chi, \tag{1.8}$$

Where N is the total number of defects on the lattice. Eq. 1.8 is know as the Poincar-Hopf theorem[13]. In the case of a simple vector field, $p = 1$. Hence a vector field on a sphere must have at least two defects of $q = 1$ so that $Q = 2$ (see Fig.1.10(a)).

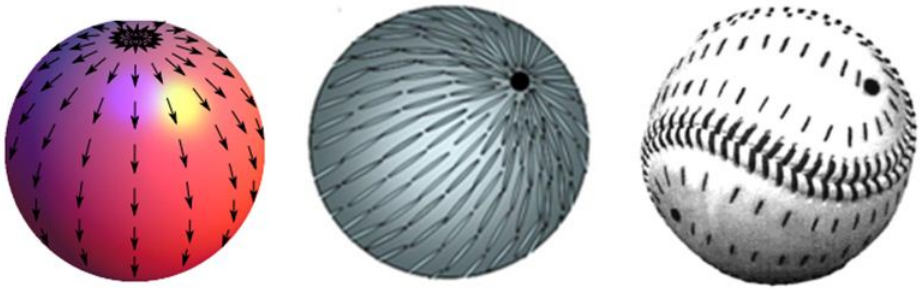

FIGURE 1.10: (Left) Vector field of a sphere. As a consequence of the Poincare-Hopf theorem, a vector field must vanish at least at two points, corresponding to the north and south pole of the sphere shown here. (center) Nematic order on a sphere: two diametrically opposite +1 defects. (Right) Nematic like texture on a baseball with four +1/2 defects located at the vertices of a tetrahedron.

In the case of nematic order, $p = 2$, since physical properties of the system remain unchanged under inversion ($\mathbf{n} = -\mathbf{n}$). Consequently, for nematic order on a sphere, the net topological charge of the defects must be 2. Theory predicts that the energetic ground state of such a system has four $+\frac{1}{2}$ defects located at the vertices of a tetrahedron[2].

[2]This means that the system is invariant under rotation by $\pi/3$

Chapter 2

Experimental Methods

2.1 Fabrication of Nematic LC Shells

Though the theoretical prediction about the tetrahedral arrangement of defects on a bi-dimensional nematic shell has been around for some years, the challenge to experimentally verify the theory had been in trying to create a shell of nematic LC that's thin enough to be considered bi-dimensional.

We set out to overcome this problem by using microfluidic techniques developed at Harvard University to create double emulsions of nematic LC[14]. A double emulsion is a drop inside a drop, and hence, the resulting structure is a shell of nematic LC.

The microfluidic device consists of two cylindrical glass capillary tubes nested within a square glass tube whose inner dimension is equal to the outer dimension of the cylindrical capillaries. This ensures that the capillaries are coaxially aligned. For convenience and greater control over the dimensions of the double emulsion, we used injection and collection tubes whose tips were tapered(see Fig.2.1(a)) by using a micropippet puller to heat the cylindrical capillary and stretch it. This process splits the capillary tube into two pieces whose tips are tapered, but sealed due to melting and re-solidification of the glass. We then use a microforge to precisely cut the tips to the desired tip diameters. Usually, the tip of the collection tube is made approximately twice as large as that of the injection tube.

The innermost fluid is pumped through the injection tube and the middle fluid is pumped through the outer coaxial region between the walls of the injection tube and the square capillary. The outer fluid is pumped through the outer coaxial region from the opposite direction, and all fluids are forced out through the collection tube. This geometry results in hydrodynamic focusing of the coaxial coflow into the collection tube[15, 16]. Inside

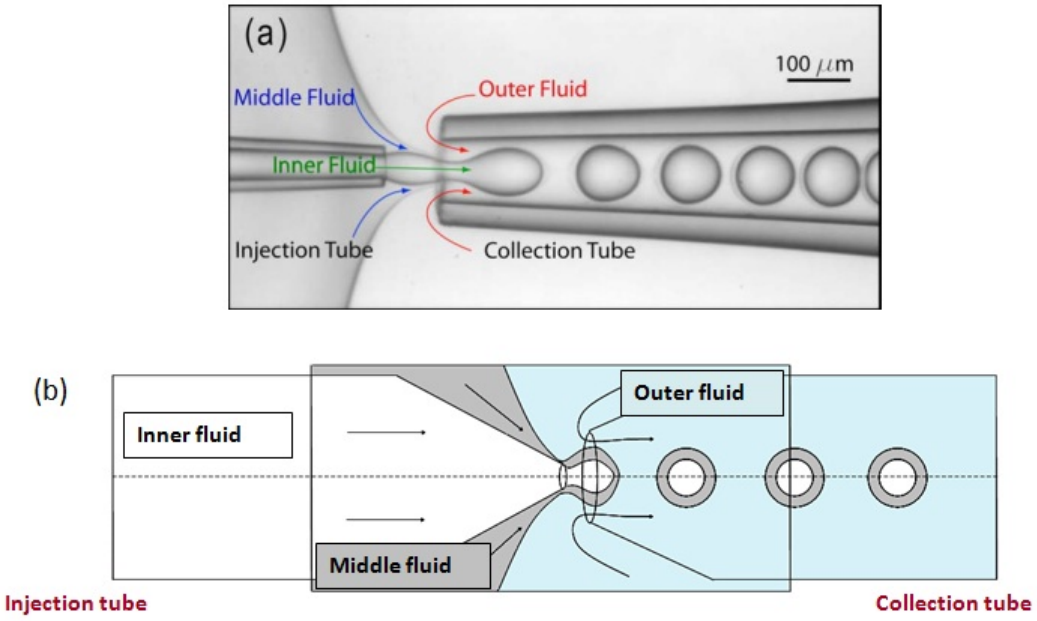

FIGURE 2.1: Microfluidic Device. (a) Micrograph of double emulsion being generated (b) Schematic of the same.

the collection tube, the jet breaks up to form drops, but as this happens, the coaxial coflow maintains its integrity, generating double emulsion droplets within the collection tube. The flow rates of the three fluids can be adjusted to generate double emulsion of different dimensions with a great amount of control.

In order to further thin the double emulsions made in this way, we use a mixture of 33 wt % of NLC and 67 wt % of chloroform. Pure nematic LC can also be used, but we use the NLC/chloroform mixture because this way, once the shells are generated, the chloroform diffuses into the continous phase, leaving behind a shell of nematic LC that is thinner than the initially fabricated shell.

Though flow rate control in the device and the use of the NLC/chloroform mixture enables us to make the shells thin, the shells are usually not thin enough to be considered spherical surfaces. To enable further thinning of the shells, we use 20 wt % salt solution as the inner fluid, and a mixture of glycerol and 20 wt % salt solution as the outer fluid. It should be noted that both these fluids contain 1 wt % of polyvinyl alcohol(PVA) to stablize the double emulsions and to enforce tangential boundary conditions for the NLC at the bounding surface[17]. Once a batch of shells of the required dimensions are collected, we dilute the continuous phase with water. This decreases the salt concentration outside the shell as compared to inside the shell, and hence, water diffuses into the shell to neutralize the osmotic pressure difference. This results in the swelling of the shell, making the shell much thinner than it initially was (Fig.2.2).

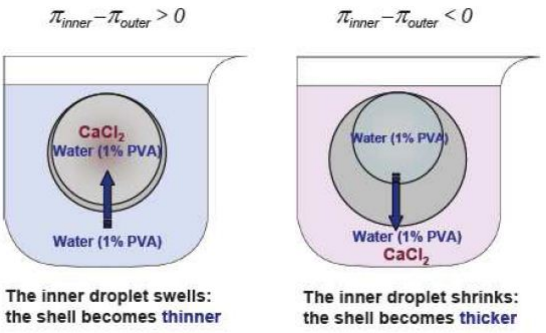

FIGURE 2.2: Osmotic pressure difference induced to make the shell thinner (left) or thicker (right).

Controlling shell thickness using osmosis has the added advantage of being performed on a cover slip while being observed under the microscope, thereby enabling us to observe the change in defect structures as the shell thickness is varied.

The microfluidic device along with the equipment required to use it is shown in Fig. 2.3.

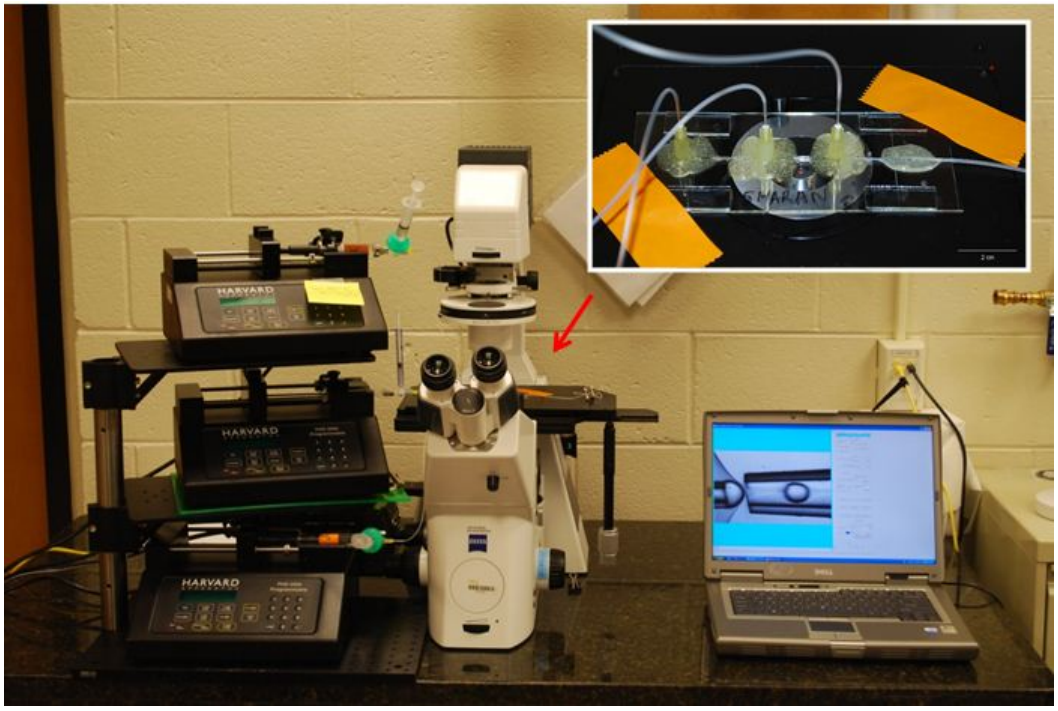

FIGURE 2.3: Microfluidic device setup: Three precision pumps are used to inject the fluid into the device shown in the inset. Visualization of the process is facilitated by the use of a high speed camera connected to the microscope.

Since the density of 5CB is more than that of water ($\delta\rho = 26.7 kg/m^3$), the aqueous inner drop of the double emulsions that we produce floats to the top, causing the shell to be thinner at the top than at the bottom as shown in Fig.2.4. This local thinning causes defects to migrate to the top to minimize the Frank-Oseen free energy. It should be noted that the local thinning effect is negligible when shells are ultrathin. The situation

is similar if $\rho_{inner} > \rho_{LC}$; in this case the bottom of the shell is thinner and the top is thicker.

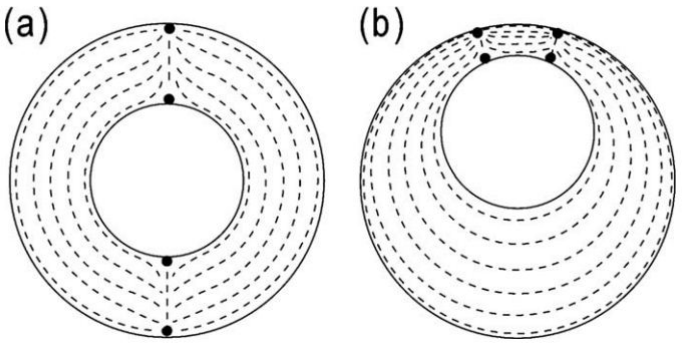

FIGURE 2.4: Nematic Shell of (a)homogenous thickness and (b)inhomogenous thickness.

Since we quantify the location of defects on shells using angular positions, we use the parameter h/R to capture the average relative thickness of the shell. Here $h = R - a$ is the average thickness of the shell, and a and R are the inner and outer radii, respectively.

The introduction of this parameter enables us to study the change in the position of the defects as a function of h/R. With this in mind, all data presented here onwards employ h/R as the *size*. Hence shells of different sizes are shells of different h/R.

To obtain statistically meaningful results for the angular separation of defects, we do ensemble averaging. Even though the microfluidic method that we use to make the shells is a highly controlled way of producing NLC shells, it is still prone to perturbations that result in the shells produced, at fixed experimentally controllable parameters like flow rates and tip diameters, to not be exactly identical. With a given sample consisting of shells that are very similar in size, we make the sample even more monodisperse by producing a distribution of the h/R values and then selecting shells that are closest together in h/R values.

2.2 Measuring shell sizes

The inner radius of a shell is measured by capturing a brightfield image of the shell with its inner edge in focus, and then using software such as *ImageJ* to superimpose a circle over the edge of the shell and reading off the radius of the circle. For measuring the outer radius, the process is repeated with the outer edge in focus. When, however, as in our case, lots of shells have to measured, this method is inefficient.

To automate this process, we wrote a MATLAB program to batch process images of shells, and output their radii. This image analysis program was written using the Generalized Hough Transform algorithm to identify the circular images of the shells and to compute their radii[18]. In addition to speeding up the process of measuring shells, this method also minimizes experimental errors. Brightfield images of a thick shell and a thin shell with circles superimposed by the program over the edges of the shells are shown in Fig. 2.5.

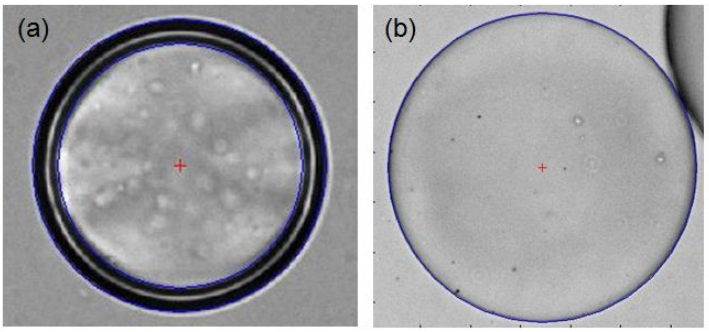

FIGURE 2.5: (a) Thick NLC shell: inner and outer edges are distinguishable (b) Thin NLC shell: indistinguishable edges

As can be seen in the Fig. 2.5(b), when the shells are very thin, the inner and outer edges of the shells are indistinguishable. In these cases, it is not possible to directly measure the thickness of the shell. We overcome this problem by making shells that are not initially too thin for their inner and outer edges to be indistinguishable, and then calculating the volume of nematic in the shell from the inner and outer radii. Once we know the volume of the shell, we make the shells as thin as we want by using osmosis. Since at this stage we know the volume and $R \approx a$, we can calculate the thickness of the shell. This technique can also be applied to distributions.

2.3 Observation of Defects

As described earlier, the optical properties of NCLs allows us to observe defects in them using cross polarized optical microscopy. A small quantity (around 200 μl) of the sample containing NLC shells dispersed in the continuous phase is placed in a cover slip with a well attached to it. The top of the well is closed with another cover slip to prevent the continuous phase from evaporating.In addition to eliminating convection, this also helps to make sure that the NLC shells in the well are completely stationary. When observed through cross polarizers, the defects and their strengths can be clearly identified.

2.4 Quantification of Defect positions

The first step in quantifying the location of defects on a shell is to find their 3D coordinates. Once these coordinates are measured, the geometry of the resulting structure can be reconstructed. The x and y coordinates are obtained by analyzing the cross-polarized image to calculate the pixel distance between the defects. We calibrate the microscope by taking an image of a diffraction grating and measuring the pixel distance between two adjacent lines. This gives us the pixel to μm conversion ratio, which we use to calculate the actual spacial distance between the defects. The z coordinate is obtained by first focusing the center of the shell, noting the reading on the fine focus knob, and then noting how many units of rotation is required to bring a defect into focus. Each division on our microscope's fine focus knob is around $2\mu m$. Once the coordinates of each defect in a shell is obtained, we calculate the angle subtended by each pair of defects with respect to the center of the shell. This angle is called the central angle (see Fig.2.6). In addition to the central angle, we use the coordinates to calculate the angular separation of each pair of defects with respect to the other defects. This angle is called the surface angle (see Fig.2.6). We automate this process over the entire ensemble of shells by using a MATLAB code.

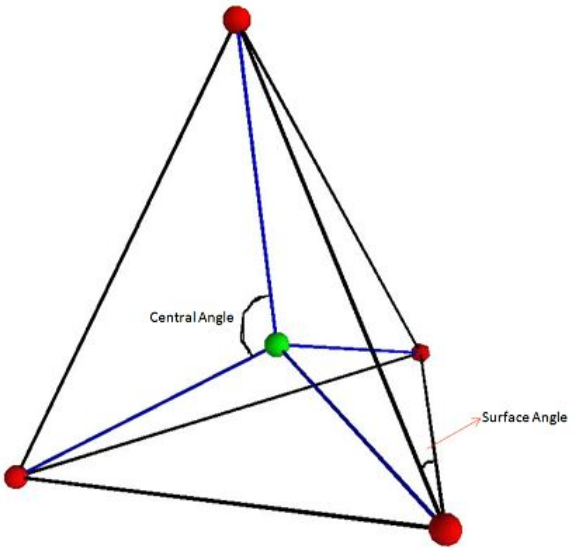

FIGURE 2.6: Schematic showing central angle and surface angle

Chapter 3

Results and Discussion

3.1 Shells with Four Defects

Using the methods described in the previous chapter, we quantify the location of the four $+\frac{1}{2}$ defects on an ultrathin shell of NLC such as that shown in Fig. 3.1.

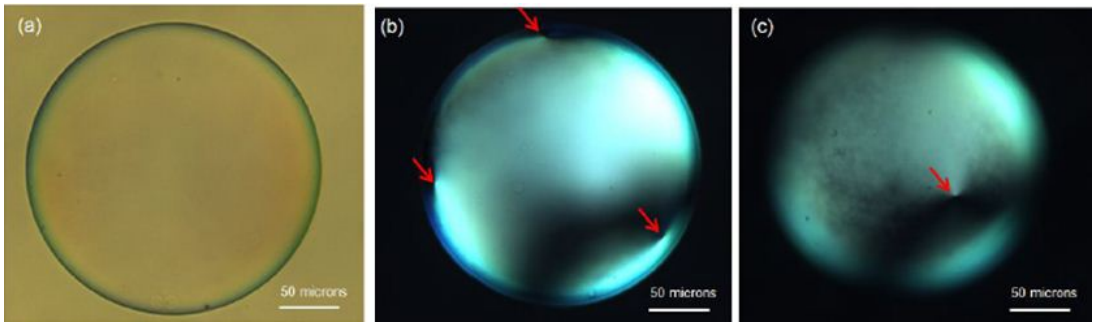

FIGURE 3.1: (a)Brightfield image of an ultrathin NLC shell (b) Cross-polarizer image of top plane showing three defects (c) Cross-polarizer image of bottom plane showing one defect. Defects are indicated by arrows.

A brightfield image of an ultrathin shell that reveals negligible thickness is shown in Fig. 3.1(a), and an image of the same shell under crossed polarizers is shown in Fig. 3.1(b). Here, the top part of the shell is in focus, and three of the four defects just happen to lie in the same plane. As we move the focus down, at the bottom part of the shell, we see another defect (Fig. 3.1(c)).

The central angle and surface angle distributions for an ensemble consisting of 30 ultrathin shells that are almost identical in dimensions is shown in Fig. 3.2.

The central angle distribution is centered at 109° with a standard deviation of 22°. Since the angle subtended at the center of a tetrahedron by any pair of its vertices is 109.47°,

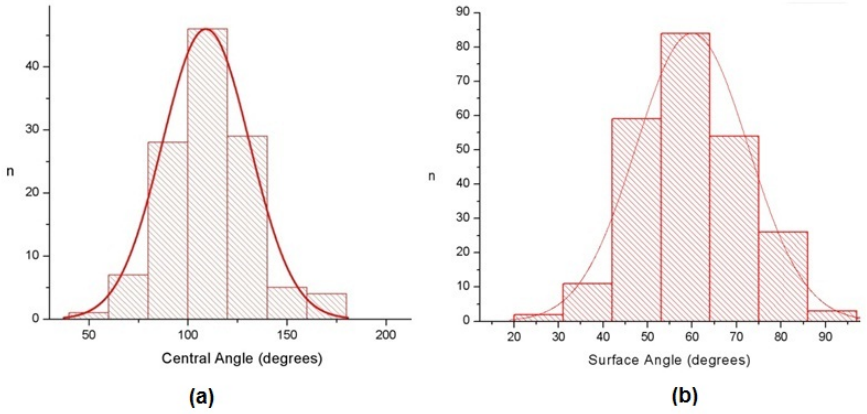

FIGURE 3.2: Distribution of central angles(a) and surface angles(b) for an ensemble of ultrathin shells.

our results tell us that the defects are indeed located at the vertices of a tetrahedron as predicted by theory.

The same inference can also be arrived at by looking at the surface angle distribution. In this case, the mean is 60° with a standard deviation of 13°. Since each face of a tetrahedron is an equilateral triangle, the surface angles should all be 60°. Our data shows that this is indeed the case, confirming the tetrahedral arrangement of the defects.

When a NLC shell is sufficiently thin, i.e. ultrathin, the shell is essentially bidimensional, and hence the defects are two dimensional disclinations. When, however, the thickness of the shell is increased, the defects become three dimensional in nature, and span the thickness of the shell. As a result, the defect becomes a *line*. Since the shells that we generate are inhomogeneous in thickness, the defects migrate towards the thinner regions of the shell until the energy associated with the defect balances their mutual repulsion. An example of how this happens is shown in Fig. 3.3. If the shells were homogeneous in thickness, then this *confinement* of defects would not occur.

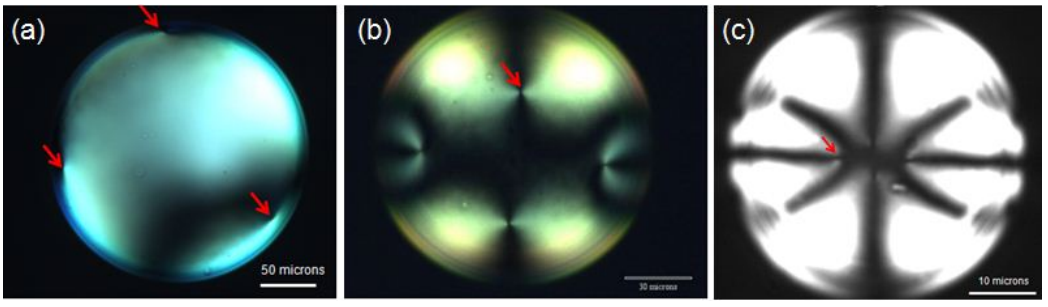

FIGURE 3.3: (a)Four +1/2 defects completely deconfined to tetrahedral structure in an ultrathin shell. Only 3 of the four defects can be seen in this image. (b) defect structure when shell is of intermediate thickness (c) most thick. Defects indicated by arrows.

In the thick shell shown in Fig. 3.3(c), the defects are arranged in a non-planar rhombic[1] structure. To substantiate this, we perform ensemble averages and obtain distributions of the central angles. The distributions for an ensemble of shells that are very thick are shown in Fig. 3.4. We initially find the distributions for the central angles subtended by each pair of defects. Since there are four defects, there are a total of six central angles that can be measured, as can be seen in Fig. 2.6. We notice that five of these distributions have peaks that are almost the same, suggesting that the corresponding angles have the same value. Combining these five distributions results in a Gaussian distribution whose standard deviation is lesser that the individual distributions, confirming that the angles do indeed have the same value.

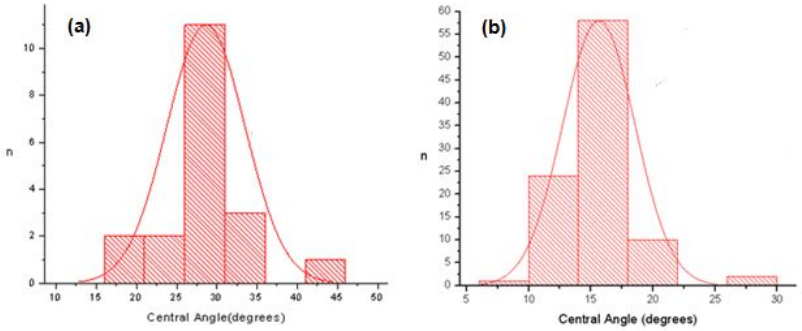

FIGURE 3.4: (a)Distribution of one of the diagonal angles (b) Distribution of the other diagonal angle and the side angle

A non-planar rhombic structure is preferred over a planar square structure because the lowering of energy brought about by two of the defects moving to a thinner part of the shell is greater than the increase in energy due to mutual repulsion. This also explains why four $+\frac{1}{2}$ defects in shells of non-negligible thickness have been observed to not be in the completely deconfined tetrahedral arrangement even when the inner drop has been experimentally made to lie at the center of the outer drop to make the shell homogeneous in thickness[19].

An intermediate configuration between the tetrahedral structure and the non-planar structure of Fig. 3.3(c) is shown in Fig. 3.3(b). This structure is also non-planar rhombic, but the defects are not as confined as those shown in Fig. 3.3(c) since this shell is much thinner. In fact, these shells are so thin that their thickness cannot be identified directly by looking at the edges of the shells. When we plotted distribution for the central angles for these shells, we noticed that the distributions are bimodal. This is explained by the fact that the sample used to produce these shells are made up of shells of two different h/R values, even though they appear to be of the same

[1]Strictly speaking, this structure is an irregular tetrahedron, but we shall refer to it as rhombic. It should be noted that for shells of intermediate thickness, the defect structure is rhombic in the sense that all their sides and one of the diagonals are equal, but the defects do not lie in the same plane.

size since they have the same R values. This was made evident when we used their volume distributions and osmosis to figure out their h/R values, as described in 2.2. The bimodal distributions for shells of intermediate thickness are shown in Fig. 3.5

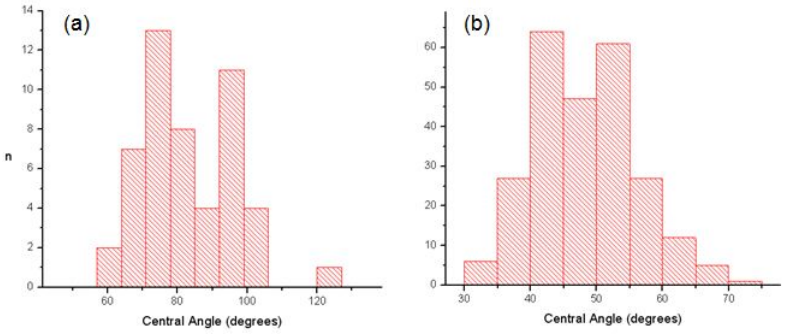

FIGURE 3.5: (a)Bimodal distribution for all the side angles and one of the diagonal angles (b)Bimodal distribution for the other diagonal angle

Once we had quantified the defect structures shown in Fig. 3.5, we[2] tracked the evolution of the defect structure of a very thin shell while deswelled using osmosis to make it ultrathin. We see that the evolution of the defect structure is continuous and implies a progressive approach of the defects towards the thinner part of the shell, as shown in Fig. 3.6. The red star points obtained from ensemble averages overlap the curve traced by the black square points obtained from the evolution of a single shell, statistically substantiating the latter results.

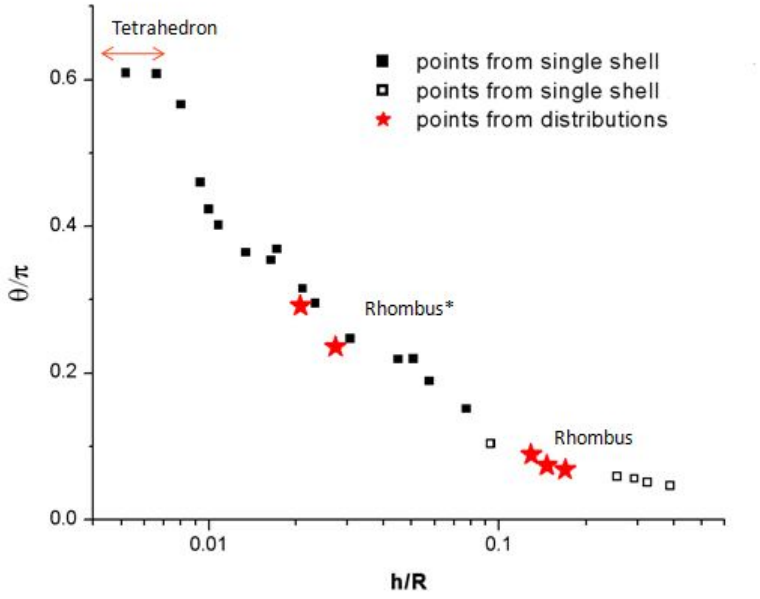

FIGURE 3.6: Evolution of the four +1/2 defect structure as a function of h/R

[2]I thank my group member, Teresa Lopez-Leon, for tracking the evolution of defects on a single shell.

Below a h/R value of 0.0067, the defects are in a tetrahedral arrangement. This, in effect, is the ultrathin regime of thickness, and in this regime, the shell can be considered bidimensional. Beyond this regime the 3D character of the shell becomes important, causing the defects to progressively migrate to the thinner part of the shell.

3.2 Shells with Three Defects

In addition to having four defects, shells of similar a and R values can have either three or two defects. This suggests that the four, three, and two defect structures are equally accessible as the shells are made and that the energy barriers between the various states are very high [20], preventing restructuring once the shells are formed.

Three defect structures are made up of two $+1/2$ defects and one $+1$ defect, as shown in Fig. 3.7(a,b). The strengths of the defects can be identified by observing how many brushes they have (see Fig. 3.7(b)). $+1/2$ defects have two brushes, and $+1$ defects have four brushes. The shell shown in this figure is relatively thick and the defects are close to the thinner part. To quantify the defect positions, we measure the angular separation of each pair of defect with respect to the third defect. We call these three surface angles $\alpha 1$, $\alpha 2$ and $\alpha 3$, as shown in Fig. 3.7(b).

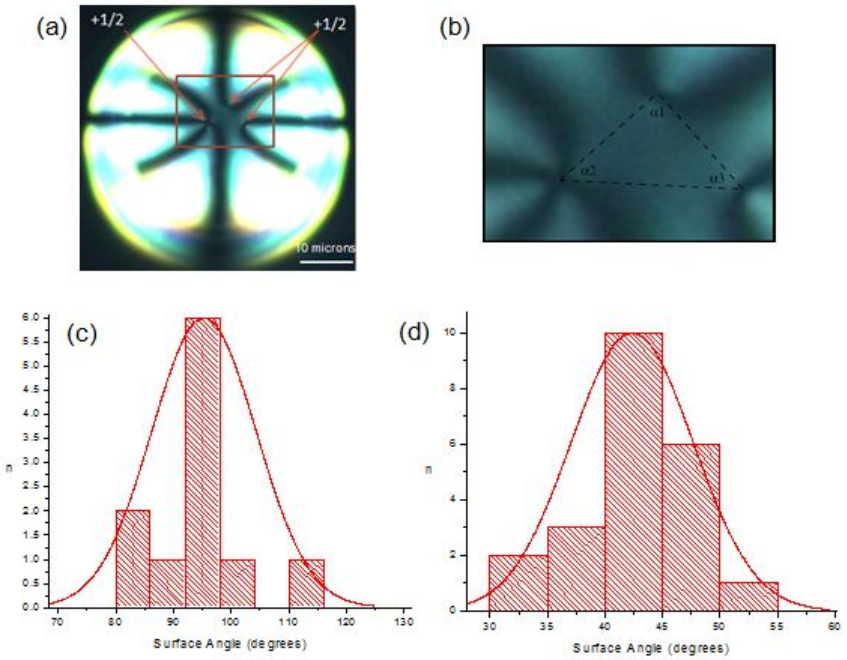

FIGURE 3.7: (a)Extremely thick shell with 3 defects (b)Blowup showing the arrangement of defects and the labeling of the surface angles (c) Distribution of $\alpha 1$ (d) Combined distribution of $\alpha 2$ and $\alpha 3$.

We note that in this configuration, the peaks of two of the three distributions were almost the same, suggesting that these angles are in fact identical. Combining these two

distributions resulted in a distribution with a spread lesser than the individual graphs, confirming that these angles are the same and giving us a more accurate estimate of the ensemble average for the angle. This indicates that the defects are located at the vertices of an isosceles triangle with $\alpha 1 = \alpha 2 \approx 42.5°$, and $\alpha 3 \approx 90°$, as shown in Fig. 3.7(c,d). Note that the +1 defect is located at one of the vertices where the angle is 42.5°. This is surprising because we expect the two +1/2 defects to be equidistant from the +1 defect. This suggest that the 3D character of the defects, which is not the same for +1 defects and +1/2 defects, affects their configuration.

For a shell of intermediate thickness such as that shown in Fig. 3.9(b), the defects are located at the vertices of a scalene triangle with $\alpha 1 \approx 79°$, $\alpha 2 \approx 56°$, and $\alpha 3 \approx 45°$, as shown by the corresponding distributions in Fig. 3.8.

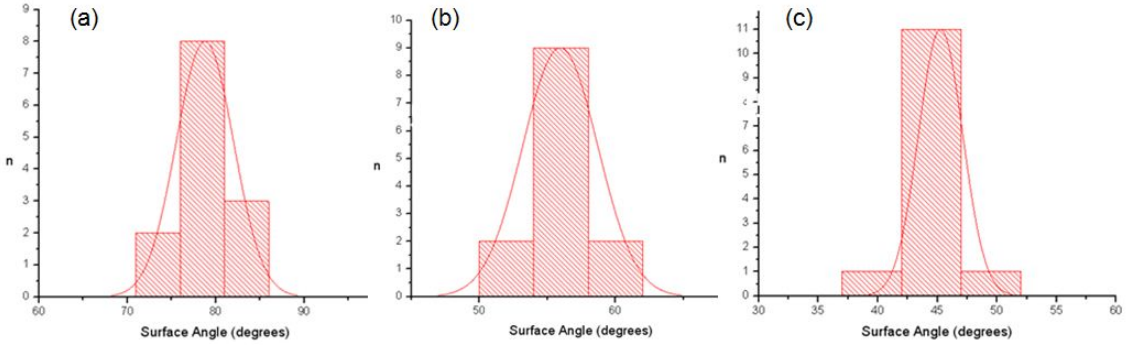

FIGURE 3.8: (a) Distribution of $\alpha 1$ (b) Distribution of $\alpha 2$ (c) Distribution of $\alpha 3$

When the shell was further thinned to make it ultrathin, we noticed that the defects are again located at the vertices of an isosceles triangle, as can be seen in Fig. 3.9(c), but unlike for the thick shell, now the +1 defect is located at the vertex that subtends the unequal angle, and hence is equidistant from the two +1/2 defects.

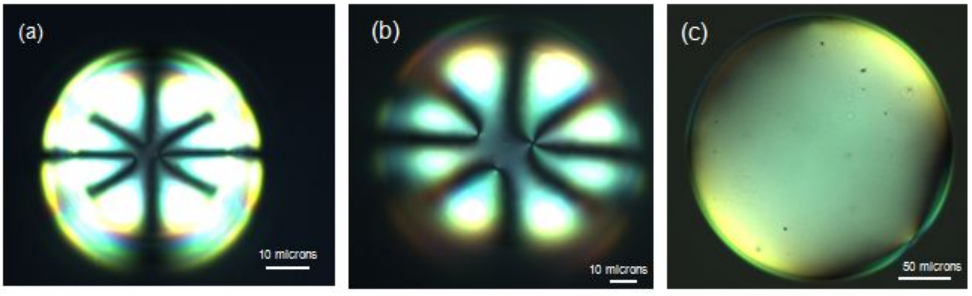

FIGURE 3.9: Evolution of the three defect structure (a) Extremely thick shell with 3 defects (b) Intermediate thickness shell with three defects (c) Thick shell with three defects.

This is as expected because topological defects in nematics interact via a long-range interaction which would tend to maximize the defect seperations. We find $\alpha 1 = \alpha 3 \approx 65°$, and $\alpha 2 \approx 50°$, as shown in Fig. 3.10.

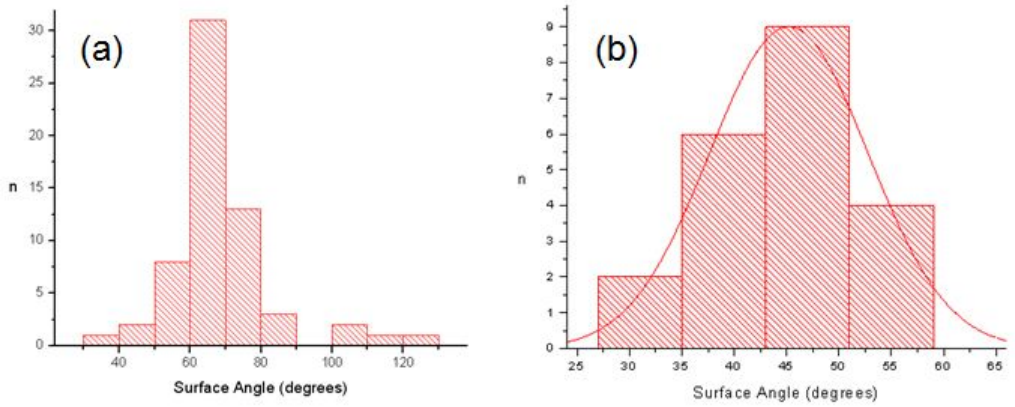

FIGURE 3.10: (a) Distribution of $\alpha 1 = \alpha 2$, and (b) Distribution of $\alpha 3$ for an ultrathin shell.

To account for the experimental results, we wrote a numerical simulation in MATLAB for three electrostatic charges of $+1/2$, $+1/2$ and $+1$ elementary unit charge interacting on a sphere, and found that the angles of the ground state isosceles structure that result in this case is $\alpha 1 = \alpha 3 \approx 65°$, and $\alpha 2 \approx 50°$, consistent with our findings.

3.3 Shells with Two Defects

In ultrathin shells with two $+1$ defects we found that the defects are located diametrically opposite to each other. Fig. 3.11(a) reveals the two defects, and Fig. 3.11(b) shows the distribution of the central angle.

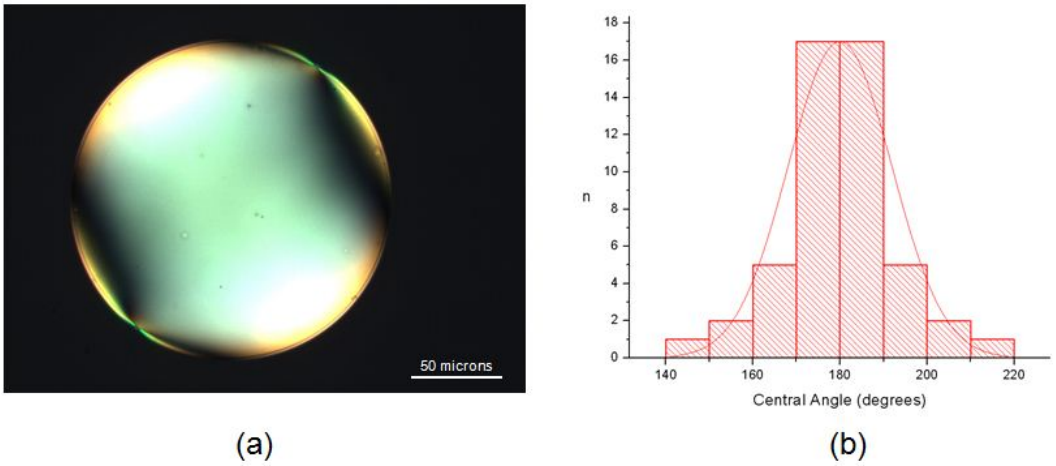

FIGURE 3.11: (a)Image of diamatrically opposite $+1$ defects on an ultrathin shell. (b)Central Angle Distribution.

3.4 Conclusion

Our results highlight the fascinating interplay between topology and nematic order of liquid crystals in determining the arrangement of defects in spherical geometries. For the first time, we have experimentally verified the tetrahedral arrangement of defects in ultrathin shells with four $q = +1/2$ defects. In addition, we have also determined the arrangement of defects in ultrathin shells with two $q = +1/2$ and one $q = +1$ defect, and in ultrathin shells with two $q = +1$ defects. In the former case, they are arranged at the vertices of an isosceles triangle, and in the latter case, they are arranged diametrically opposite each other.

These three configurations are the starting point to a rich behavior in the possible defect configurations, where the key is the thickness inhomogeneity. As the shell becomes thicker, the defects progressively confine in the thinner part of the shell.

Bibliography

[1] TC LUBENSKY and J PROST. ORIENTATIONAL ORDER AND VESICLE SHAPE. *JOURNAL DE PHYSIQUE II*, 2(3):371–382, MAR 1992. ISSN 1155-4312.

[2] David R. Nelson. Towards a tetravalent chemistry of colloids. *Nano Letters*, 2 (10): 1125–1129, 2002.

[3] G.P.Crawford and S.Zumer. *Liquid Crystals in Complex Geometries*. Francis and Taylor London, 1996.

[4] A. Fernandez-Nieves, V. Vitelli, A. S. Utada, D. R. Link, M. Marquez, D. R. Nelson, and D. A. Weitz. Novel defect structures in nematic liquid crystal shells. *PHYSICAL REVIEW LETTERS*, 99(15), OCT 12 2007. ISSN 0031-9007. doi: {10.1103/PhysRevLett.99.157801}.

[5] R Moessner and AR Ramirez. Geometrical frustration. *PHYSICS TODAY*, 59(2): 24–29, FEB 2006. ISSN 0031-9228.

[6] Rmy Mosseri. Geometrical frustration and defects in condensed matter systems. *Comptes Rendus Chimie*, 11(3):192 – 197, 2008. ISSN 1631-0748. doi: DOI:10.1016/j.crci.2007.03.019. URL http://www.sciencedirect.com/science/article/B6X18-4PT2FS3-1/2/f7f4475274d5b9e0ad6f1da960f06049. Morphogenese et cristaux liquides.

[7] Prost J. de Gennes P.G. *Physics of Liquid Crystals*. Clarendon Press, 1993.

[8] N.D. Mermin. The topological theory of defects in ordered media. *Rev. Mod. Phys.*, 51(3):591–648, 1979.

[9] G. Friedel. Dislocations. *Pergamon Press*, 1964.

[10] S.D. Sharma and editors A. Pinczuk. Perspectives in quantum hall fluids. *John Wiley and Sons*, 1997.

[11] N. Turok I. Chuang, R. Durrer and B. Yurke. Cosmology in the laboratory: Defect dynamics in liquid crystals. *Science*, 251:1336–1342, March 1991.

[12] Maurice Kleman and Oleg D. Lavrentovich. *Soft Matter Physics: An Introduction*. Springer; 1 edition, October 1, 2002.

[13] H. poincar, j. math. pures appl. 1, 167 (1885); h. hopf, math. ann. 96, 427 (1926).

[14] A. S. Utada, E. Lorenceau, D. R. Link, P. D. Kaplan, H. A. Stone, and D. A. Weitz. Monodisperse Double Emulsions Generated from a Microcapillary Device. *Science*, 308(5721):537–541, 2005. doi: 10.1126/science.1109164. URL http://www.sciencemag.org/cgi/content/abstract/308/5721/537.

[15] I. G. Loscertales, A. Barrero, I. Guerrero, R. Cortijo, M. Marquez, and A. M. Ganan-Calvo. Micro/Nano Encapsulation via Electrified Coaxial Liquid Jets. *Science*, 295(5560):1695–1698, 2002. doi: 10.1126/science.1067595. URL http://www.sciencemag.org/cgi/content/abstract/295/5560/1695.

[16] D. R. Link, S. L. Anna, D. A. Weitz, and H. A. Stone. Geometrically mediated breakup of drops in microfluidic devices. *Phys. Rev. Lett.*, 92(5):054503, Feb 2004. doi: 10.1103/PhysRevLett.92.054503.

[17] A.A.Sonin. *The Surface Physics of Liquid Crystals*. Gordon and Breach, London, 1995.

[18] Linda Shapiro and George Stockman. *Computer Vision*. Prentice-Hall, Inc., 2001.

[19] A. Fernandez-Nieves, V. Vitelli, A. S. Utada, D. R. Link, M. Marquez, D. R. Nelson, and D. A. Weitz. Novel defect structures in nematic liquid crystal shells. *Phys. Rev. Lett.*, 99(15):157801, Oct 2007. doi: 10.1103/PhysRevLett.99.157801.

[20] V Vitelli and D. R. Nelson. Nematic textures in spherical shells. *Phys. Rev. E*, 74 (2):021711, Aug 2006. doi: 10.1103/PhysRevE.74.021711.